Dual Vortex Structure Shedding from Low Aspect Ratio, Surface-mounted Pyramids

Robert J. Martinuzzi
Department of Mechanical and Manufacturing Engineering
Schulich School of Engineering
University of Calgary
Calgary, Alberta, Canada T2N 1N4
Email: rmartinu@ucalgary.ca

ABSTRACT

The flow around surface-mounted, square-based pyramids, of apex angles ranging from 5° to 90°, placed in a thin boundary layer with one face normal to the on-coming flow was investigated for Reynolds numbers of 10 000 to 150 000 using surface pressure measurements, Laser Doppler and Particle Image Velocimetry as well as oil-film surface flow patterns. Based on the periodicity of the surface pressure on the pyramid side faces, four distinct shedding regimes were identified: constant local Strouhal number, discrete cellular, low aspect ratio and suppressed. Closer inspection of the low aspect ratio regime indicates that two distinct vortical structures are shed at the same frequency. Vortices are shed alternately from opposing faces in the obstacle base region, while hairpin vortices are shed in-phase and are most easily observed near the tip region of the pyramid. It is further shown that the existence of these structures is consistent with the mean surface flow topology observed in the wake and side faces of the obstacles.

INTRODUCTION

Observations of periodic vortex shedding from low aspect ratio, surface-mounted bluff bodies reveal a complex phenomenology difficult to reconcile under a single physical model. Sakamoto and Arie (1983) investigated the flow in the wake of surface-mounted vertical cylinders of square and circular cross-section. They reported that above a critical height-to-width (aspect) ratio, which depends on the on-coming boundary layer thickness, vortices were shed alternately from opposing sides, similarly to the classical von Karman vortex street. For smaller aspect ratios, arch (or hairpin) type vortices were shed symmetrically about the centre-line. Similar shedding patterns were observed by Savory and Toy (1986) in the wake of surface-mounted hemispheres. Studies performed on finite aspect ratio, vertically mounted circular cylinders (Okamoto and Sunabashia, 1992; Sumner *et al*., 2004) found the co-existence of vortex shedding near the body-wall junction (base) and in-phase vortex structures near the free-end. The wake of tapered obstacles, such as cones (Vosper *et a*l., 1999) or triangular plates (Castro and Watson, 2004) displays a similar behaviour for apex angles ranging from 12° to 75°.

It has been suggested (cf. Sumner et al., 2004) that the downwash generated at the free-end of the obstacle leads to the formation of tip vortices, which locally suppress the vortex formation process on the side faces of the obstacle. This explanation, however, is difficult to reconcile with a topologically consistent flow model as it tacitly implies the existence of open-ended vortex structures. Furthermore, its generalisation to tapered geometries is difficult since, for cones and triangular plates, an upwash is observed at the tip, rather than a downwash, and the tip entrainment area vanishingly small.

EXPERIMENTAL DETAILS

The flow around low aspect ratio, surface-mounted pyramids placed in a thin boundary layer with one face normal to the free stream was investigated for Reynolds numbers ranging from 10 000 to 150 000, based on the free stream velocity, U_∞, and the pyramid height, h. The experimental set-up and nomenclature are schematically summarized in Fig. 1. Tests were conducted for individual pyramids of apex angles ζ = 5°, 8°, 12°, 15°, 30°, 45°, 60°, 75° and 90°. Pyramids of height h = 0.050m were tested in a 0.46m × 046m cross-section, suction wind tunnel, while pyramids of h = 0. 914m were tested in a 1.5m × 2.4m boundary layer wind tunnel test section. In all cases, the boundary layer thickness was approximately 0.1h, the free stream turbulence less than 1% and the blockage ratio was less than 2%, such that no correction was applied to the measurements. Surface pressure measurements were made simultaneously from thirty uniformly distributed pressure taps on the opposing faces of the pyramid and on additional pressure taps placed in the ground plate in the obstacle wake.

Sampling rates ranged from 400Hz to 1500Hz to maintain a resolution of at least 12 points per shedding cycle. The maximum vortex shedding frequency recorded was 100Hz. The pressure-tapping-system response was flat to approximately 200Hz. The free stream velocity was monitored using a single hot-wire anemometer (HWA) sampled simultaneous with the pressure measurements. HWA measurements of the velocity fluctuations at different heights above the ground plane at x/h = 1.8 and 2.4 were also made for several pyramids.

Mean surface flow patterns were obtained using an oil-film technique for all cases. The pressure measurements were complemented by two-component Laser Doppler Velocimetry (LDV) and Particle Imaging Velocimetry (PIV) measurements for selected cases. Further details are provided in Martinuzzi and AbuOmar (2003).

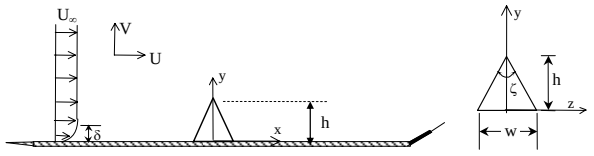

Figure 1: Schematic representation of the flow configuration and nomenclature.

RESULTS AND DISCUSSION

The periodic nature of the surface pressure measurements and flow field behaviour were similar over the entire range of Reynolds numbers tested. Generally, transition to turbulence of the shear layers occurs rapidly near the leading edges of the pyramid such that the wake flow is fully turbulent. Based on the periodicity of the surface pressure fluctuations observed on the side faces of the pyramids, it will be shown that the nature of vortex shedding can be classified in four regimes as a function of the pyramid apex angle: constant local Stouhal number ($\zeta < 7°$), discrete cellular shedding ($8° \le \zeta \le 12°$), low aspect ratio ($15° \le \zeta < 75°$) and suppressed shedding regimes ($\zeta > 75°$). The flow field for the low aspect ratio regime will be discussed in greater detail by combining the results of several different measurement techniques.

Classification of Shedding Regimes

For very shallow pyramids ($\zeta > 80°$), no evidence of periodicity in the surface pressure fluctuations on the side faces of the pyramids could be observed. The relative inclination of the shear layers separating from the highly tapered leading edges is sufficiently large to inhibit the coupling of the opposing shear layers. As observed by Martinuzzi and AbuOmar (2003), pyramids with an apex angle of $\zeta = 90°$ do not show any periodicity on the side faces when mounted with one face normal to the flow (angle of attack of 0°). However, when the pyramid is placed at an angle of attack of 22.5° or 45°, periodicity is again observed on the side faces and the wake flow.

For mildly tapered pyramids ($\zeta < 7°$), changes in the periodicity of the surface pressure fluctuations on the pyramid side faces are similar to those observed in Fig. 2 for the pyramid $\zeta = 5°$. A strong, constant frequency cell is observed in the pyramid base region, which extends from the junction with the ground plate to approximately 0.38h. Above $y \approx 0.41h$, a strongly modulated periodic signal is observed resulting in a broad spectral energy distribution. The central (peak) frequency associated with this distribution lies along a constant local Strouhal number, based on U_∞ and the local obstacle width. A similar behaviour has been reported for mildly tapered cones and triangular plates (cf. Vosper *et al*., 1999; Castro and Watson, 2004).

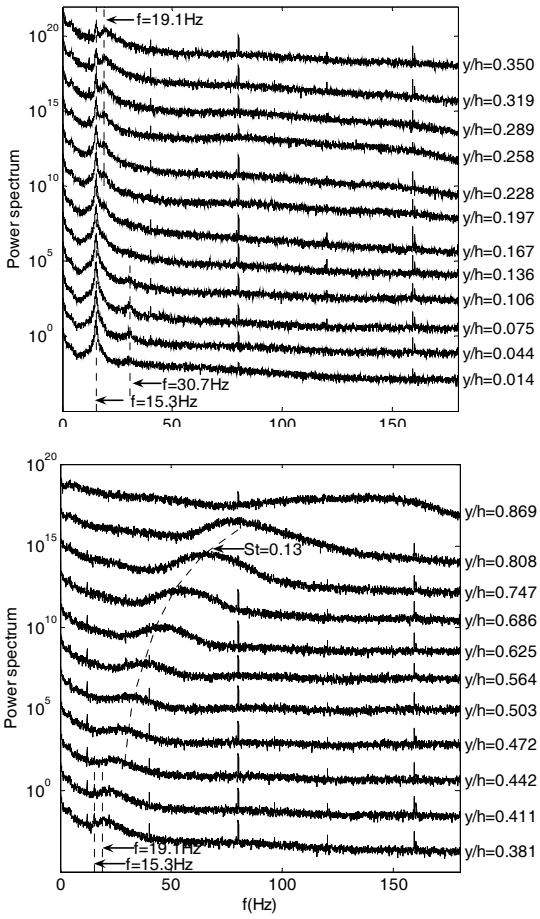

Figure 2: Power spectral density function of the pressure fluctuations along the side face of a pyramid $\zeta = 5°$. Spectra are off-set by a factor of 10 for clarity.

For the pyramids $\zeta = 8°$ and 12°, spectra of the fluctuations of the surface pressure from the side faces of the pyramid clearly show two distinct constant-frequency cells. A typical example is provided in Fig. 3 for the pyramid $\zeta = 8°$. In the base region, pressure fluctuations on opposite faces are again 180° out-of-phase, suggesting the alternate shedding of vortices. On the upper half of the pyramid, however, the fluctuations on opposing faces are nearly in-phase. Figure 4 shows the cross-correlation between a pressure tap on the ground plate and the velocity for locations above the pressure tap. The pressure tap and HWA were located roughly 1.8h downstream of the tip and half-way between the plane of symmetry (z = 0) and the base

edge of the pyramid (i.e. one quarter of the base width). Typically, the pressure fluctuations on the ground plate at this location are approximately between 45° and 90° out-of-phase with the velocity fluctuations associated with the shedding cell near the ground plate (y/h < 0.5) and nearly in-phase with the fluctuations in the upper cell (y/h > 0.5).

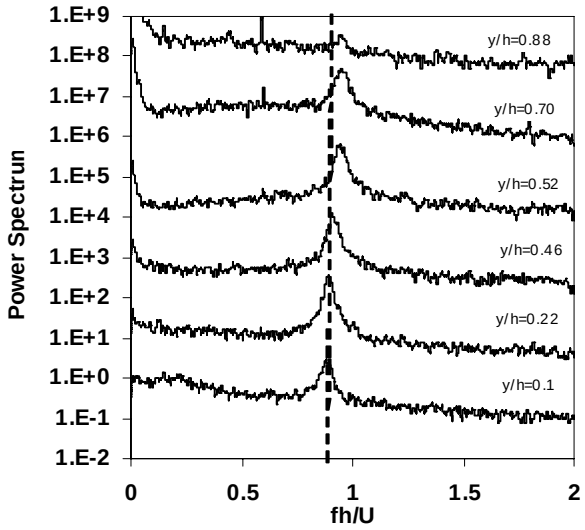

Figure 3: Power spectral density function of the pressure fluctuations along the side face of a pyramid $\zeta = 8°$. Spectra are off-set by a factor of 10 for clarity.

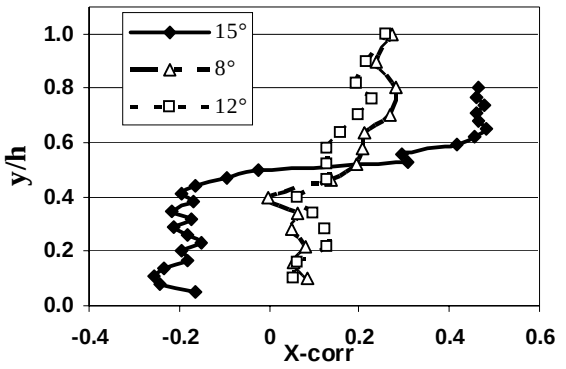

Figure 4: Cross-correlation coefficient for surface pressure on the ground plate and velocity in the wake of the pyramid.

The behaviour of the surface pressure fluctuations on the side faces of the pyramid are qualitatively similar for $\zeta = 15°$ to $\zeta \sim 75°$. Sample power spectra at different locations along the side faces are shown for $\zeta = 15°$ and $\zeta = 45°$ in Fig. 5. A single constant-frequency cell is observed to span the side face, although the periodicity of the signal becomes difficult to recognize near the tip. Closer inspection of the dynamic behaviour of the pressure fluctuations, however, reveals some important differences between the base and tip regions. Figure 6 shows a composite of the fluctuating component of the pressure time series over the two side faces for the pyramid $\zeta = 15°$.The grey scale levels correspond to the fluctuation amplitude. In the base region (y/h < 0.5), the intensity of the pressure fluctuations is highest and nearly constant. The frequency of the dominant fluctuations is very regular and these oscillations are 180° out-of-phase on opposite faces.

As the pyramid tip is approached, the amplitude of the fluctuations is increasingly modulated. Near the tip, the fluctuation amplitude appears to display an irregular beat pattern. Although the dominant frequency does not change (see Fig. 5), it becomes increasingly difficult to identify from the time series. While for y/h < 0.5 the fluctuations on the same side of the pyramid are in-phase, for y/h > 0.5, there is a small, but increasing phase difference with height. Furthermore, in the tip region (y/h > 0.8), the fluctuations on the opposite sides of the pyramid are in-phase.

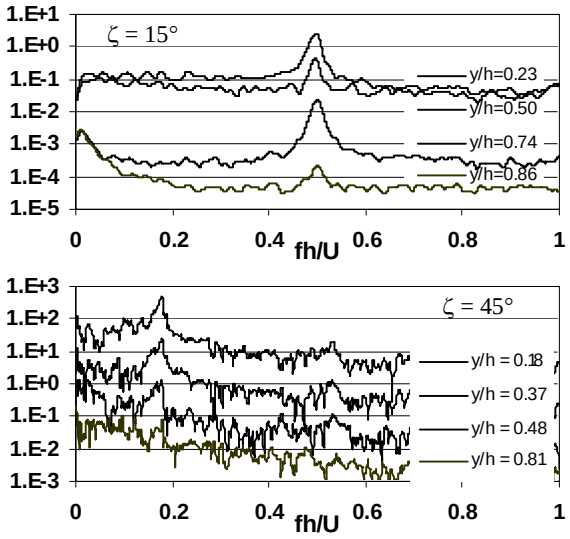

Figure 5: Power spectral density function of the pressure fluctations along the side face of pyramids $\zeta = 15°$ and 45°.

These observations are qualitatively valid for all pyramids in this regime, although the extent of the base region increases further from the ground plate towards the tip as the apex angle increases. For example, Fig. 7 shows the cross-correlation function for selected points along the side faces for the pyramid $\zeta = 45°$. The base region extends to approximately y = 0.65h.

Considering the pyramid $\zeta = 15°$, it seen from Fig. 4 that the cross-correlation coefficient, between the surface pressure measured on the ground plate in the wake of the pyramid and the velocity measured at different locations above the pressure tap, is negative below y/h ~ 0.5 and positive above. Figure 8 shows the associated cross-correlation functions. While the frequency does not change, there is a change in the phase relationship consistent with the behaviour of the surface pressure fluctuations on the pyramid side faces as described in relation to Fig. 6.

Its is difficult to attribute the change in phase relationship along the height of the frequency to a bending or distortion of a single vortex since, based on the results of Fig. 4 and 8, the change occurs abruptly and the velocity-pressure cross-correlations clearly fall into two categories. It is possible, however, to attribute these changes to the shedding of two different structures at the same frequency.

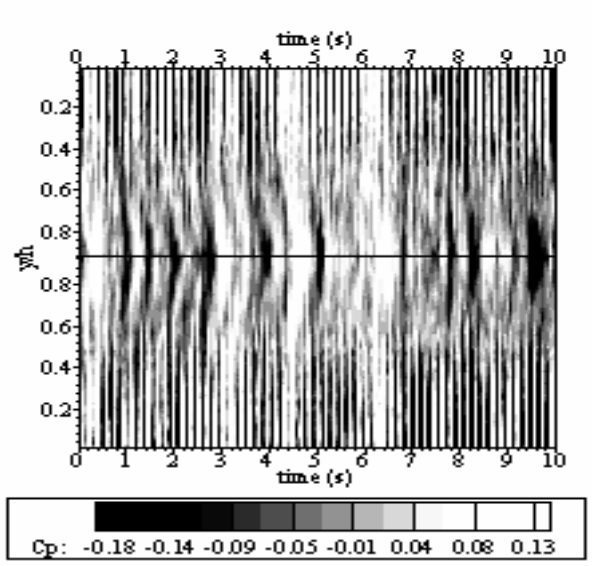

Figure 6: Time series of the fluctuating component of the surface pressure on the side face of the pyramid $\zeta = 15°$.

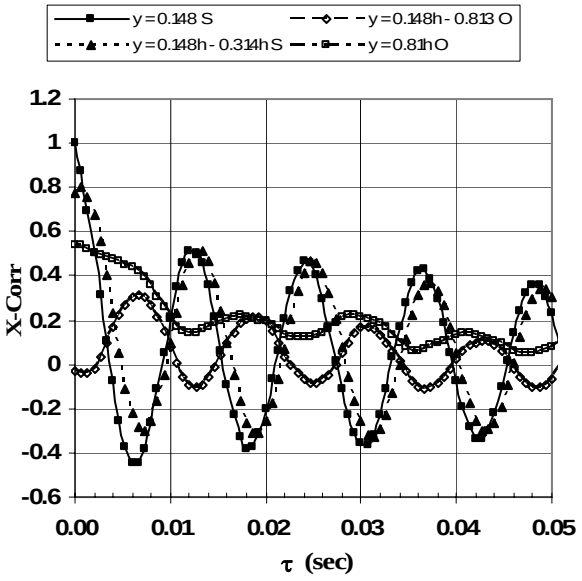

Figure 7: Cross-correlation coefficients between surface pressure measurements along the centre line of the side faces for pyramid $\zeta = 45°$. "S" tap locations on the same side, "O" on opposing sides.

Flow field for low aspect ratio pyramids

The existence of two vortex structures being shed at the same frequency is difficult to verify based on surface pressure measurements or single-point velocity measurements. However, by combining velocity field measurements and surface flow pattern visualization results, a topologically consistent flow model for dual vortex shedding can be developed which can account for observed flow features that cannot exist with a single vortex shedding model.

The mean surface flow patterns on the side face of pyramid $\zeta = 60°$, obtained with an oil-film technique, are shown in

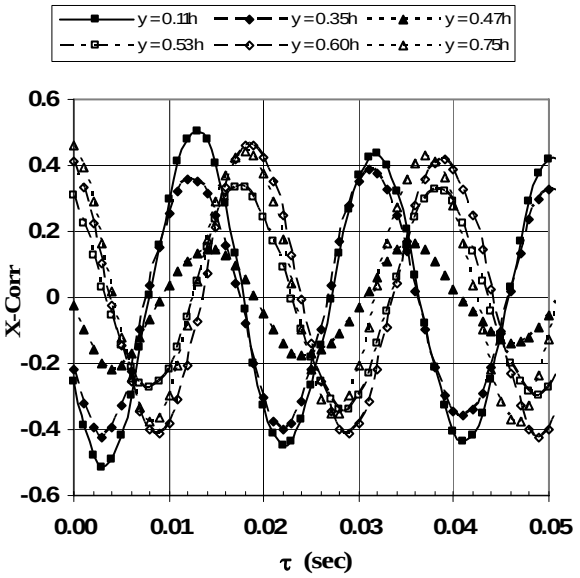

Figure 8: Cross-correlation coefficients between velocity fluctuations and surface pressure. Surface pressure measured in pyramid $\zeta = 15°$ wake at x/h = 1.8 and z/h = 0.04 (pyramid edge at z/h = 0.8). Velocity measurements were made at locations above this point.

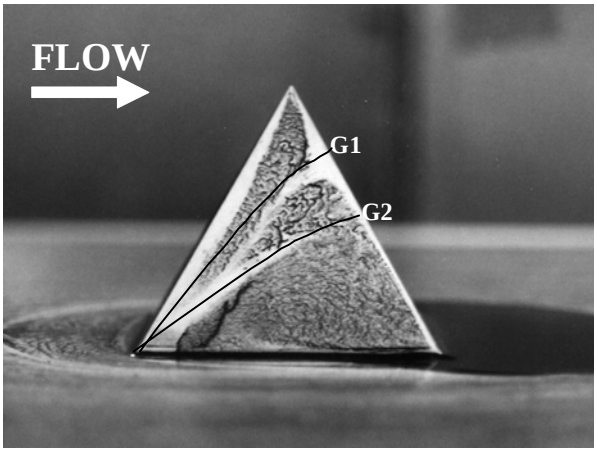

Figure 9: Surface flow patterns on the side faces for a pyramid $\zeta = 60°$ obtained using an oil-film technique (Reynolds number of 33 000 based on U_∞ and h).

Fig. 9. The pigment accumulation lines **G1** and **G2** are associated with co-rotating vortex pairs originating at the leading edge corner of the pyramid-ground plate junction. A counter rotating vortex is induced between **G1** and **G2** to satisfy kinematic constraints.

The mean surface flow patterns on the side face of pyramid $\zeta = 60°$, obtained with an oil-film technique, are shown in Fig. 9. The pigment accumulation lines **G1** and **G2** are associated with co-rotating vortex pairs originating at the leading edge corner of the pyramid-ground plate junction. A counter rotating vortex is induced between **G1** and **G2** to satisfy kinematic constraints.

The velocity field along the side faces of the pyramid is shown in Fig. 10. Consistent with the topology deduced from Fig. 9, the lines **G1** and **G2** are divergent and convergent bifurcation lines, respectively. The vortex formed between the leading edge and **G1** feeds the large vortex core downstream of the tip. By symmetry, the vortex forming on the opposing face between the leading edge and **G1** also extends to the wake vortex, thus forming a hairpin structure.

Below the line **G2**, the surface pressure fluctuations are highly coherent: the amplitude down to the obstacle junction is nearly constant, in-phase with a very regular periodicity. These fluctuations are out-of-phase with those on the opposite face. Above this pigment line, the fluctuations there is a decrease in the correlation coefficient, the amplitude and frequency are more strongly modulated and the phase changes. Above the line **G1**, the fluctuations on the opposing faces are nearly in-phase.

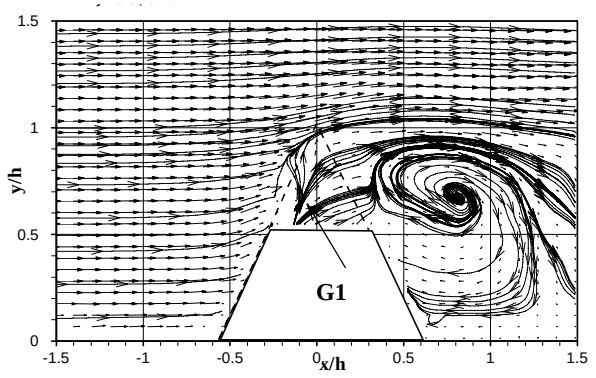

Figure 10: Mean velocity field and stream-traces obtained with PIV in the xy-plane (z/h=0.2) for ζ=60°, α=0° and Reynolds number of 33 000.

Evidence of the dual structure vortex shedding events at the same frequency can be found by viewing instantaneous velocity measurements in cross-sectional (x-constant) planes in the wake. Representative examples are shown in Fig. 10 for the plane x/h = 1.8 for the pyramid ζ = 60°. Since the hairpin structure sheds in-phase and the base vortices shed alternately from the opposing faces, three distinct and periodically recurring events should be observed. Between shedding events of the hairpin vortex, it is possible to observe instances when only one of the alternating vortices is present (Fig. 10a). Due to the velocity gradient normal to the ground plate, the shed vortices are rotated and stretched in the streamwise direction. It is thus possible to observe three vortices (the two contributions of the hairpin vortices and one of the alternating vortices), as shown in Fig. 10b, or all four vortices, albeit at different stages of their respective shedding cycles (Fig. 10c). As expected, in the mean these vortical structures are not apparent downstream of the obstacle leeward base region.

The surface flow patterns and a schematic of the topological interpretation are provided in Fig. 12. A sketch of the deduced vortex skeletons is shown in Fig. 13. The lines $\mathbf{B_{P3}}$ and $\mathbf{B_{N3}}$ correspond to the pigment lines **G1** and **G2** in Fig. 9. The node N_3 corresponds to the mean attachment point in the wake. The node N_2 is is associated with the recirculation vortex observed in the wake. The flow regions below **G2** (or $\mathbf{B_{N3}}$) and above $\mathbf{N_2}$ are simply connected. This observation is interpreted to imply that the flow regions on the side faces below **G2** and above $\mathbf{N_2}$ are part of the alternately shedding vortex identified as **AV** in Fig. 13. The shed vortex **AV** extends downstream and its rotation would induce a flow towards the plane of symmetry (z = 0) and an upwash in the z-plane flow. However, as indicated by the oil-film results of Fig. 12, there is a positive bifurcation line along z = 0 (i.e. the flow moves outward), resulting in a negative bifurcation line $\mathbf{B_{N2}}$. This bifurcation line is diverging, implying a sustained mass flux towards the ground plate (i.e. a downwash in the plane z = 0). A bound hairpin vortex, as appears from the mean field velocity measurements and is labelled **HP** in Fig. 13, can account for the existence of the node $\mathbf{N_3}$, but not the continuous mass flux required to generate the bifurcation line $\mathbf{B_{N2}}$. However, if the hairpin vortex, or part thereof, sheds, the extensions (**HPe** in Fig. 13) would provide for a sustained mass flux and be consistent with the observed wake flow topology.

CONCLUDING REMARKS

It has been proposed that, for low aspect ratio pyramids of apex angles ζ 15° to 75°, a dual vortex shedding model can explain the constant frequency and shedding-phase relationships observed on the obstacle side faces and wake. A vortex cell at the base of the obstacle sheds alternately from the opposing sides, while a hairpin structure sheds in-phase near the tip. This model is consistent with the observed mean flow topology in the wake on the ground plate and along the plane of symmetry (z = 0). The pressure perturbations caused by the alternately shedding cell may trigger the shedding of the hairpin vortex and thus explain the constant frequency observed on the side faces. However, the downstream interactions of the shed vortices and how the topological constraints on the vorticity field are satisfied has not been elucidated.

REFERENCES

Castro, I. P.,, and Watson, L., 2004, "Vortex shedding from tapered, triangular plates: taper and aspect ratio effects," *Experiments in Fluids*, Vol. 37, pp/ 159-167.

Martinuzzi, R. J., and AbuOmar, M., 2003, "Study of the Flow Around Surface-Mounted Pyramids," *Experiments in Fluids*, Vol. 34, pp. 370-389.

Okamoto, S., and Sunabashia Y., 1992, "Vortex Shedding from a Circular Cylinder of Finite Length Placed on a Ground Plane", *Journal of Fluids Engineering*, Vol. 114, pp. 512-521.

Vosper, S. B., Castro, I. P., Snyder, W., and Mobb, S. D., 1999, "Experimental Studies of Strongly Stratified Flow Past Three-Dimensional Orography," *Journal of Fluid Mechanics*, Vol. 390, pp. 223-249.

Sakamoto, H., and Arie, M., 1983, "Vortex shedding from a rectangular prism and a circular cylinder placed vertically in a turbulent boundary layer", *Journal of Fluid Mechanics*, Vol. 126, pp. 147-165.

Savory, E., and Toy, N., 1988, "The Separated Shear Layers Associated With Hemispherical Bodies in Turbulent Boundary Layers," *Journal of Wind Engineering and Industrial Aerodynamics*, Vol. 28, pp. 291-300.

Sumner, D., Heseltine, J. L., and Dansereau, O. J. P., 2004, "Wake structure of a finite circular cylinder of small aspect ratio", *Experiments in Fluids*, Vol. 37, pp.720-730.

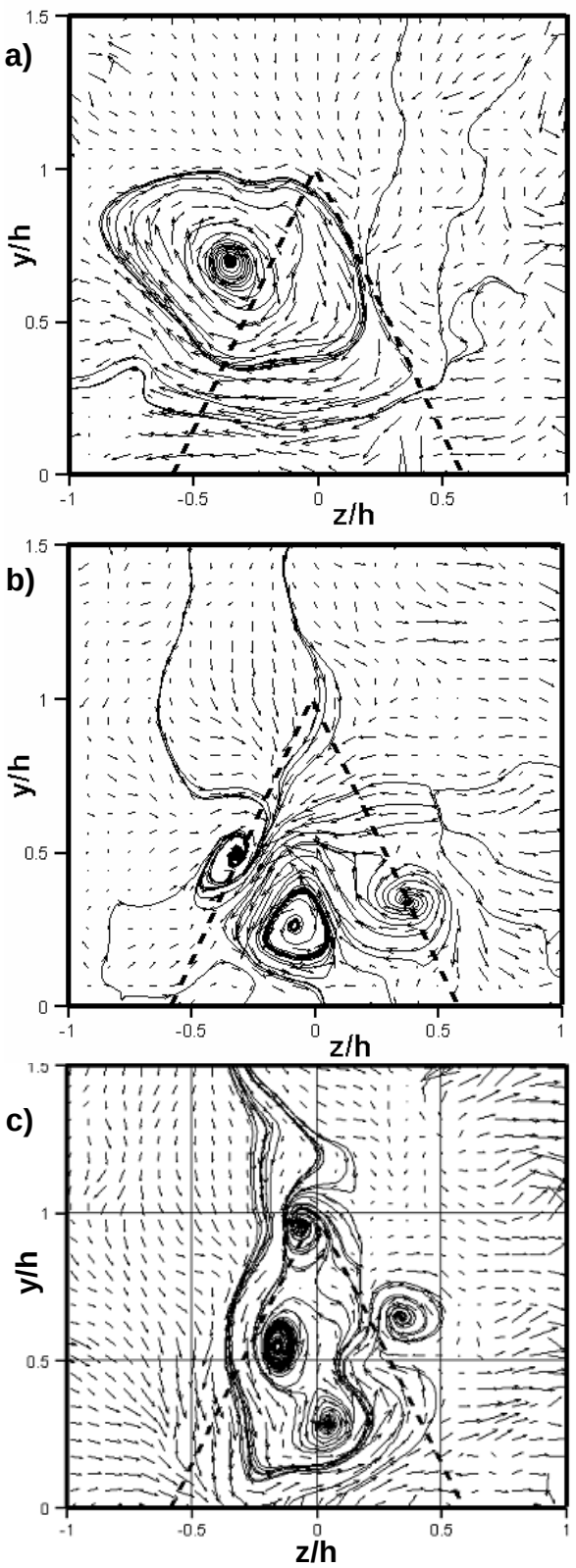

Figure 11: Instantaneous PIV images of the velocity vectors at a location x = 1.8h downstream of the tip for the pyramid ζ = 60° (Reynolds number of 20 000).

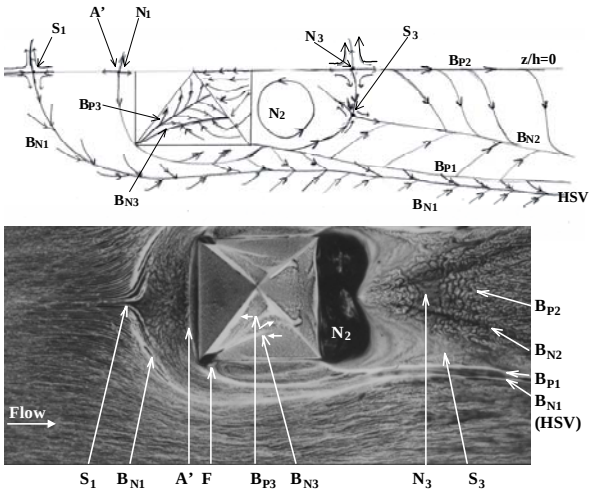

Figure 12: Schematic representation (top) of the topological interpretation of the oil-film surface flow patterns (bottom) for pyramid ζ = 60°.

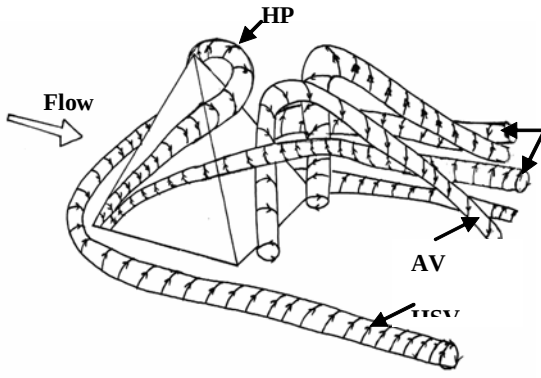

Figure 13: Vortex skeleton sketch for the flow around low aspect ratio (ζ = 15° - 75°) pyramids.